energies

MDPI

Article

Grid-Forming Operation of Energy-Router Based on Model Predictive Control with Improved Dynamic Performance

Mahdieh Najafzadeh[1], Natalia Strzelecka[2]*, Oleksandr Husev [1], Indrek Roasto [1], Kawsar Nassereddine [3], Dmitri Vinnikov [1] and Ryszard Strzelecki [4]

[1] Department of Electrical Power Engineering and Mechatronics, Tallinn University of Technology, Tallinn 19086, Estonia. mahdieh.najafzadeh@taltech.ee, indrek.roasto@ieee.org, oleksandr.husev@taltech.ee, dmitir.vinnikov@taltech.ee;
[2] Faculty of Electrical Engineering, Gdynia Maritime University, 81-225 Gdynia, Poland, n.strzelecka@we.umg.edu.pl;
[3] Faculty of Engineering, Lebanese University, Lebanon; nassereddinejana@gmail.com;
[4] Faculty of Electrical and Control Engineering, Gdańsk University of Technology, 80-233 Gdańsk, Poland, ryszard.strzelecki@pg.edu.pl;

Abstract: The focus of this study is on the grid-forming operation of the Energy Router (ER) based on Model Predictive Control (MPC). ER is regarded as a key component of microgrids. It is a converter that interfaces the microgrid (s) with the utility grid. The ER has a multiport structure and bidirectional energy flow control. The ER concept can be implemented in Nearly Zero Energy Buildings (NZEB) in order to provide flexible energy control. A concept where the ER works as a single grid-forming converter is proposed. The challenge is to keep the predefined reference voltage and frequency inside the NZEB in all possible modes, including the idle operation mode, current sources, and nonlinear load control. To gain stability and output voltage quality, the MPC is proposed. The design of the modified MPC algorithm with improved dynamics performance is explained. PLECS software is utilized to verify the proposed algorithm.

Keywords: energy router; current sources; nonlinear load; grid-forming control, bidirectional power flow control; model predictive control

Citation: Lastname, F.; Lastname, F.; Lastname, F. Title. *Energies* **2022**, *15*, x. https://doi.org/10.3390/xxxxx

Academic Editor: Firstname Lastname

Received: date
Accepted: date
Published: date

1. Introduction

The steadily increasing penetration of renewable energy sources (RESs) in the utility grid is a current trend [1], [2], which, in turn, is a source of many technical challenges to be overcome. The voltage/frequency disturbances caused by the chaotic nature of RES in the utility grid are widely known.

The solution is to shift the responsibility to the local prosumer. Accordingly, in many countries, governments have set strict regulations on grid energy injection. It consists of the limitation of the injected power into the grid produced by RES in local households. Near Zero Energy Building (NZEB) is a concept providing a reduction in energy consumption in households. It is achieved in several ways, including energy-saving technologies, modern heating systems, and modern power electronics facilities. New power electronics facilities ensure zero energy consumption by means of energy flow control between RESs, storage batteries and loads. Priorities announced are drifting from mass RESs used for grid balancing.

A more recent concept is the so-called smart communities, which take advantage of the Smart Grid (SG), allowing effective demand-side management. SGs require general-purpose power electronic converters (both in dc and ac), micro-storage systems installed at the residential level, advanced metering infrastructure, and optimal use of information

and communication technology. In this regard, the trend goes toward the concept of energy routers (ERs) or hubs [3].

The concept of ER, introduced by the NSF FREEDM Systems Center in 2010 [2], introduces an SST-based ER concept and describes the IoE architecture. The further concept development for microgrids application is addressed in many papers. Complementary energy exchange by means of ER between neighboring microgrids is addressed in [4]. The

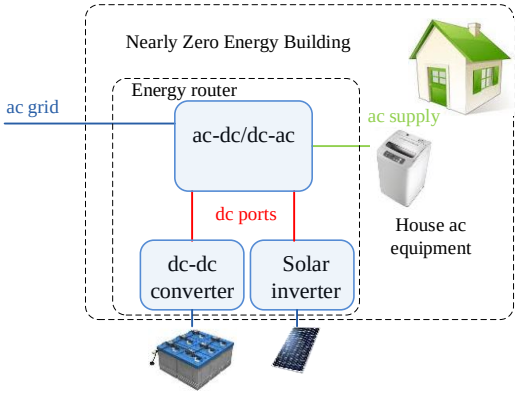

Figure 1. Energy router for NZEB.

control strategy of ER inside a microgrid with different energy sources, loads and battery ES is studied in [5]. Work [6] studied utilization of a hybrid converter as an ER in a case of dc nanogrid. Finally, paper [7] is devoted to the ER as a power management tool in case of low-voltage residential application. The further extension of this approach consists in ER utilization for NZEB concept. It has to provide flexible energy management in case of different loads, energy sources, and battery storage. Also, in advance to the grid-connected mode, the islanded mode, when the main grid is disconnected have to be realized. As a conclusion, the NZEB corresponds to the hybrid nanogrid [8], [9], while the goal of the ER is to keep stable output voltage all operation modes. Active and reactive power control, voltage control, current control, and protection functions are just a few of the active functions that an ER could have.

Figure 1 shows a single-phase multiport converter topology that is selected to realize the interface between external grid and internal load. Inherently, it has dc and ac terminals, that make it similar micro-and nanogrids converters [10]. Two dc-dc interface converters allow to connect energy storage and local energy generation source. Also dc loads can be considered [11]. The output ac port is directly connected to the house appliances. Appliances in in the NZEB are considered as "grid followers," only. At the same time, it is well-known that diferent types of load have to be considered including light load and non-linear loads. Basic operation modes of the considered ER are described in [12]. This work studies in detail the quality of the grid-forming operation.

2. Conventional Grid-Forming Control Systems and Problem Definition

Figure 2 shows the electrical circuit diagram of the ER. The measured signals are marked in red. One of the conventional control systems of the ER is shown in Figure 3. It has a conventional Phase-Locked Loop (PLL) block that provides synchronization to the primary grid [13]. The traditional Second Order Generalized Integrator (SOGI) regulator is used [14]. The grid side reference current is derived by means of a simple proportional-integral (PI) controller in combination with the instantaneous value of the output current. It provides the instantaneous power balance between the output side and the grid side, which in turn mitigates power ripple across the dc-link capacitor and improves the dynamic of the system. Finally, a conventional proportional-resonant (PR) controller is used for grid current control. Thus, the grid-side control operation is ensured (Figure **3**a.).

The PR controller is a key element of the discussed grid-side control system. In order to provide the proper dynamic, it has to be the fastest and properly tuned chain in the control loop [15].

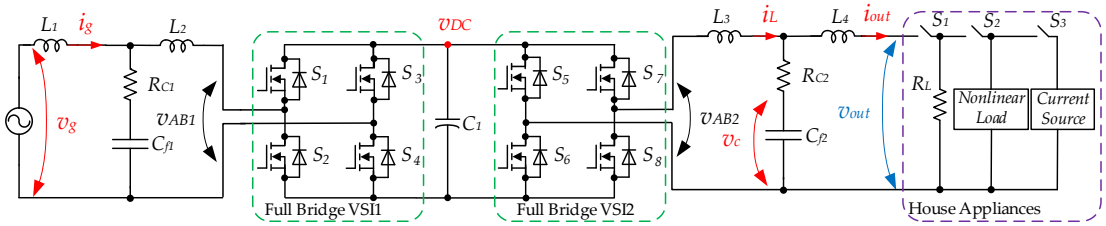

Figure 2. Back to back mode circuit diagram of the proposed energy router.

The output control has a more complex structure. The classical definition of the grid-forming operation is derived from the microgrid application and has high-level and low-

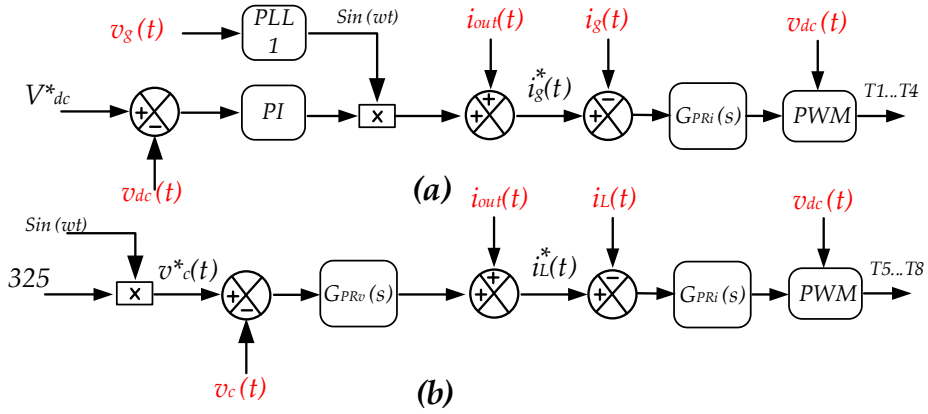

Figure 3. The conventional control system structure of the ER primary grid-side VSI1 control (a) and output side grid-forming VSI2 control (b).

level control components. The low-level algorithm has to provide the output voltage according to the reference value. One of the examples of the output voltage control structure is illustrated in Figure 3b. The initial goal of the output side controller is to provide sinusoidal output voltage under any output load. As a result, a consumer recognizes it as a normal grid. It typically has current and voltage control loops [16–20].The internal structure can be different. In the three-phase system, the dq rotating frame is often used, while resonant controllers are mostly used for a single-phase system. In both cases, the main attention should be paid to the stable operation of the system. The current control loop is usually tuned as a fast control loop, while the voltage control loop has a damped dynamic.

The high-level algorithm provides the power sharing control in the case of several power sources working in parallel. First and foremost, it is achievable through Droop control [21–25]. It is a well-known and verified approach.

The Virtual impedance [26], [27] method and its derivation can also be applied for this purpose. Finally, a relatively novel approach based on the synchronverter concept was proposed in [28–30].The goal of a high-level algorithm is to provide different amplitudes and frequencies of the reference voltage across the filter capacitor. It enables stable operation of the microgrid. However, it is out of scope for this work.

In the classical approach, the voltage at the Point of Common Coupling (PCC) is not under direct control. It is assumed that only linear loads with sinusoidal current sources can be connected to the PCC. At the same time, it is obvious that this assumption is not

acceptable in household applications where ER is connected to different low power loads and current sources. I think it's clear that the PCC is getting higher harmonics from things like solar microinverters and other nonlinear loads and current sources like this.

This paper is about how to make the voltage shape in the PCC better when the ER is used with different loads and current sources.

3. Grid-Forming Operations Based on Indirect Model Predictive Control

Model Predictive Control (MPC) is a well-known approach in power electronics from the 1980s. Despite the complexity of the MPC which imposes limitations on its utilization in power electronics, the progress of computational resources makes it more and more feasible for industrial applications [31]-[33]. According to the most recent research, it can be used in a variety of power electronics fields [34]-[42].

Figure 4 shows the proposed control system. The control system for the primary side of the ER is shown in Figure 4a. Only one modification concerns an additional PLL block. It provides a pure sinusoidal reference current that is equal to the fundamental harmonic of the output current. It will provide only sinusoidal grid current under any shape of the output current. All non-active harmonics will be circulated between the DC-link and the secondary side of the ER.

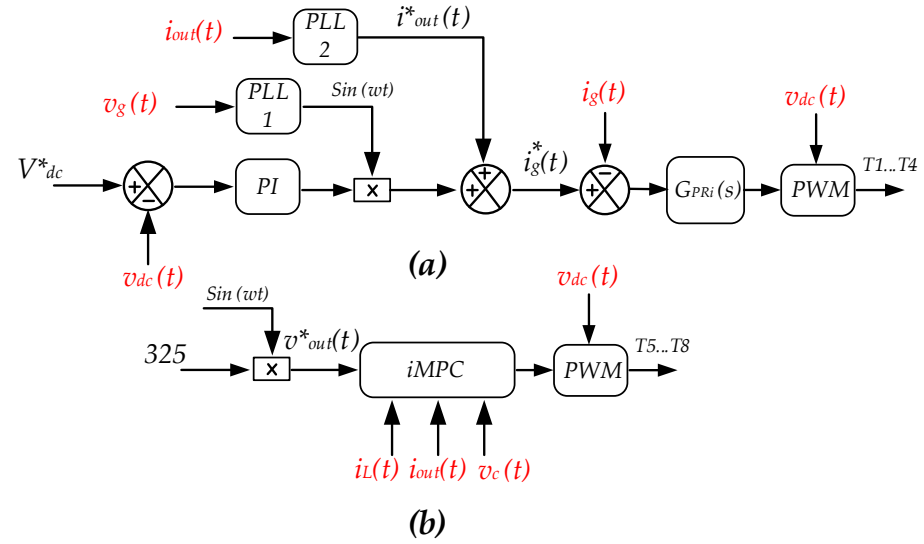

Figure 4. The proposed control system structure of the ER primary grid-side VSI1 control (a) and output side grid-forming VSI2 control (b).

Figure 4b shows the part of the control system that is in response to the grid-forming operation. In a very general case, the MPC says what the control action should be by trying to minimize a cost function that describes how the system should work.

The proposed approach was partially studied in [43] for the unidirectional power flow control mode. In our case, the main goal of the proposed control system is to keep the output voltage shape according to the reference sinusoidal signal under any type of load or current source that can be connected from the house side. As different from the classical approach, where only the voltage across the filter capacitor is controlled, MPC allows control of both the voltages across the capacitor and the output voltage even without direct measurement of the last value. It turns out that, in our case, the cost function J is defined as:

$$J\,[d]\ = k_{out}|\Delta v_{out}(n+1)| + k_c|\Delta v_c(n+1)| + .. + k_{out}|\Delta v_{out}(n+p)| + k_c|\Delta v_c(n+p)| \quad (1)$$

It contains an error of the voltage across the filter capacitor and an error of the output voltage, along with corresponding weighting coefficients. Also, it has p elements that are defined by horizon prediction. The function quantizes estimations of different summarized outputs and capacitor voltage errors. Each of those estimations correspond to the possible scenario d, which could occur at the prediction horizon.

The measurement system gives the dc-link voltage, the voltage across the filter capacitor and currents in the inductors. If you want to do any more calculations, you need to use the indirect MPC and the dynamic model of the system shown in Figure 5.

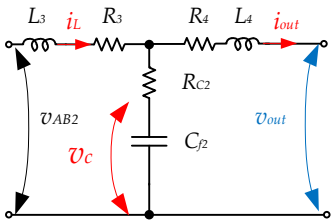

Figure 5. The dynamic model of the secondary side part of the ER used for iMPC.

The dynamic system is represented by the continuous vector of the measured parameters:

$$x(t) = [\, i_L(t), i_{out}(t), v_c(t)]^T, \tag{2}$$

After the measured signal discretization, the discontinuous set of the measured values is derived:

$$x(\mathrm{i}) = [\, i_L(i), i_{out}(i), v_c(i)]^T, \tag{3}$$

After obtaining the measured values, the first step is to calculate the voltage at the PCC point based on a simple equation:

$$v_{out}(n\,) = v_c(n\,) - \big(i_L(n) - i_{out}(n)\big) \times R_{C2} - \frac{L_3}{T_S}(i_{out}(n) - i_{out}(n-1)) - R_4 \times i_{out}(n), \tag{4}$$

where T_S is the sampling time, L_3, L_4, C_{f2} are parameters of the output filter, R_3, R_4, R_{C2} are parasitic resistances.

In order to calculate the grid current value during the next samples in the discrete-time domain:

$$x(n\ +1) = F \cdot x(n) + G\ u(n), \tag{5}$$

$$\mathrm{u}(n)\ =\ [\, v_{AB}(\mathrm{n}), v_{out}(\mathrm{n})\,]^T \tag{6}$$

where F and G are matrices that correspond to the dynamic model of the system and sampling frequency:

$$F = \begin{bmatrix} \mathrm{f}_1 & \mathrm{f}_2 & \mathrm{f}_3 \\ \mathrm{f}_4 & \mathrm{f}_5 & \mathrm{f}_6 \\ \mathrm{f}_7 & \mathrm{f}_8 & \mathrm{f}_9 \end{bmatrix}, \tag{7}$$

$$G = \begin{bmatrix} g_1 & 0 \\ 0 & g_4 \\ 0 & 0 \end{bmatrix}, \tag{8}$$

$$f_1 = 1 - (R_3 + R_{C2})\frac{T_S}{L_3}; f_2 = \frac{R_{C2}T_S}{L_3}; f_3 = -\frac{T_S}{L_3}; \tag{9}$$

$$f_4 = \frac{R_{C2}T_S}{L_4}; f_5 = 1 - (R_4 + R_{C2})\frac{T_S}{L_4}; f_6 = \frac{T_S}{L_4}; \tag{10}$$

$$f_7 = \frac{T_S}{C_{f2}}; f_8 = -\frac{T_S}{C_{f2}}; f_9 = 1; \tag{11}$$

$$g_1 = \frac{T_S}{L_3}; g_4 = -\frac{T_S}{L_4}, \tag{12}$$

The approach proposed gives us a reference output voltage in the PCC. To make sure the control system works properly, the voltage across the capacitor is set as follows:

$$v_c^*(t) = v_{out}^*(t) - (i_L(t) - i_{out}^*(t)) \times R_{C2} + L_4\frac{d}{dt}i_{out}^*(t) + R_4 \times i_{out}^*(t), \tag{13}$$

In the further step, the voltage across capacitor of the output filter is calculated as a function of the applied inverter voltage. The same concerns the output voltage in the PCC, which can be estimated similar to Eq. (4). As a result, the proposed control system keeps under control the capacitor voltage and the voltage in the PCC, taking into account the difference between them.

Finally, possible errors are calculated:

$$\Delta v_{out}(n+1) = v_{out}(n+1) - v_{out}^*(n+1);\ \Delta v_c(n+1) = v_c(n+1) - v_c^*(n+1); \tag{14}$$

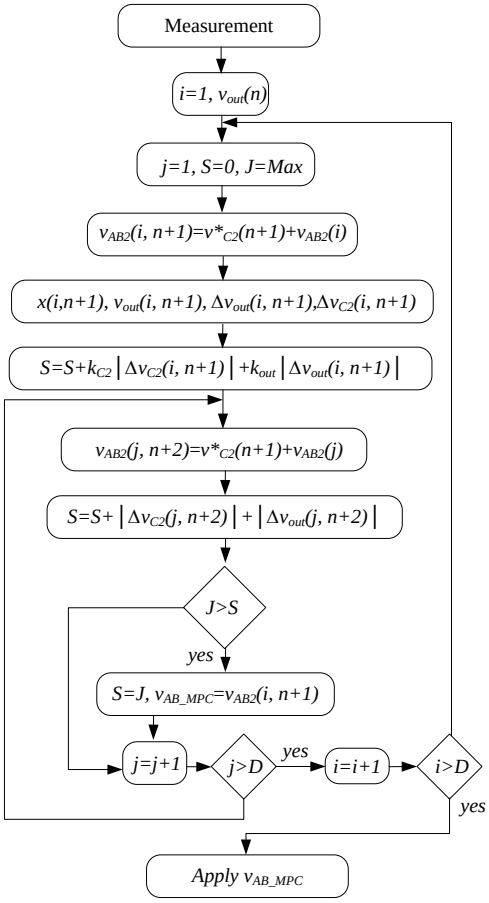

Figure 6. The flow chart diagram of the proposed iMPC in the case of p =2.

The flow chart diagram for the case $p = 2$ is shown in Figure 6. Firstly, the variables are measured, and then the output voltage is estimated.

Based on this estimated state, the predicted state of the system at $n + 1$ for all the possible output inverter values v_{AB2} combinations is calculated.

It should be mentioned that, in any case, the output inverter voltage is expected to be close to the sinusoidal reference signal. $v_{AB2(i)}$ is an example of a possible reference voltage that could be used to figure out the cost function:

$$v_{AB2}(n+1) = v_c^*(n+1) + \Delta v_{AB2}(i), \tag{15}$$

Finally, the combination of voltages on the output inverter that minimizes (1) is stored and will be used at the start of the next test.

4. Optimal Parameters Selection

The main criterion for the quality evaluation of the output voltage is the THD. At the same time, from the description above, it is evident that the resulting THD depends on the horizon prediction p, weighting coefficients, and the voltage quantizing d. Due to the nonlinearity of the control, the most suitable tuning approach is achieved by simulation. In this work, the PLECS simulation tool was used as the simulation environment.

The parameters of the prototype are shown in Table 1. They are used for simulation and experimental tests.

First of all, based on previous research [43], it is assumed that the horizon prediction $p = 2$ is optimal. Increasing p even more won't make a big difference in THD, but it will make the calculations a lot more complicated. According to Eq. (15), the output voltage value is selected close to the present reference voltage value with respect to voltage deviations. During each sampling, five possible output voltage deviation values are considered and verified one by one. This number is constant from sample to sample, which is limited by the calculation resources. But the possible minimum and maximum values can be different:

$$-\Delta v_{AB2\_max} < \Delta v_{AB2}(i,d) < \Delta v_{AB2\_max}, \tag{16}$$

Table 1. Components and parameters of the ER.

Parameter	Value3
Input RMS ac voltage V_{IN}	230 V
Output ac RMS voltage V_{OUT}	230 V
Output power	0.3-3.6 kW
Dc-link capacitor C_1	0.8 mF
Grid side inductor filter L_1	0.6 mH
Grid side second inductor filter L_2	1.44 mH
Grid side capacitor filter C_{f1} R_{C1}	3 μF, 0.8 Ohm
Output side inductor filter L_3	1.44 mH
Output side second inductor filter L_4	0.6 mH
Output side capacitor filter C_{f2} R_{C2}	9.6 μF, 0.8 Ohm
Switching frequency f	25 kHz
Sampling frequency f	25 kHz

It is well known that the voltage difference between the filter capacitor and the PCC is defined by the parasitic resistance R_4 (Figure 5), inductance L_4 and current. The maximum and minimum voltages that can be applied to the inverter can be flexible and changed a little bit based on the peak current.

In conclusion, the most significant parameters to be evaluated are the weighting coefficients. The idea of these coefficients consists of a priority setting between the quality of the output capacitor voltage and the quality of the PCC voltage. On the one hand, it is evident that the PCC is more important than the voltage across the capacitor, which is an internal parameter. But, this is a parameter that can be directly measured, and direct control of it could improve both the capacitor and the PCC.

A simulation was performed to study the influence of these coefficients. Figure 7 shows the simulation results in the case of. It means that only the quality of the capacitor voltage is taken into account in the cost function estimation. At the very beginning, the DC-link is charged and a 529 W simple resistive load is connected at 0.25 s. At the moment of 0.35 s, the nonlinear 180 W load is connected. To emulate a highly nonlinear load, a resistor with a half-bridge diode with an LC filter is assumed. It can be seen that at the resistive load, both the capacitor and the PCC voltage have good shape without significant distortions. At the nonlinear load connection, both voltages have distortions. But it is evident that the capacitor voltage is less distorted. The grid current is also distorted by the nonlinear load connection.

The opposite situation is shown in Figure 8. In this case, the predicted capacitor voltage is not taken into account in the cost function estimation. It can be seen from Figure 8 that with a simple resistive load, the quality of the PCC voltage and the capacitor voltage is good, but the situation changes under a nonlinear load. Both shapes are distorted more compared to Figure 7 results. However, the THD of the grid current remains constant.

The simulation results of different coefficients k_{out}, k_c show the influence of the weighting coefficients k_{out}, k_c on the THD of output voltage and capacitor voltage. It is assumed that $k_{out} + k_c$=1 under nonlinear load. The results show that different values of k_{out} and k_c have no significant impact on THD, but lower k_{out} improves the output voltage and capacitor voltage quality.

Figure 9 shows the simulation of the whole system under different load conditions. It includes an idle mode, a simple resistive load, and a nonlinear load. They are utilized in this case. This figure demonstrates the steady state pictures with a better resolution as well as the dynamic behavior of the main grid, ac output, and the capacitor. This figure shows that the proposed iMPC can work because the THD of the output voltage and the grid current are in the range that they should be.

The next scenario is to evaluate the iMPC performance in the opposite power flow in a low-power solar microinverter connection. Figure 10 demonstrates the simulation results in idle mode and with a current-source connection. The results confirm the good performance of the iMPC in terms of grid-forming. However, the high THD of grid current implies the necessity of improvement in current control on the VSI1 side. The last case is the most complex and reveals a problem with any grid configured by power electronics. The high switching frequency current harmonics fluctuate between the ER and the microinverter.

It can be seen that the proposed control approach is capable of keeping sinusoidal voltage in the PCC under any type of load that can be connected on the house side. Moreover, it underlines that the ER requires modification on the VSI1 side to keep an acceptable quality of the injected current on the local grid under any load from the consumer side. Finally, bidirectional operation is possible without significant PCC voltage distortion. It lets you use renewable energy sources in your home without having to connect them to the electricity grid

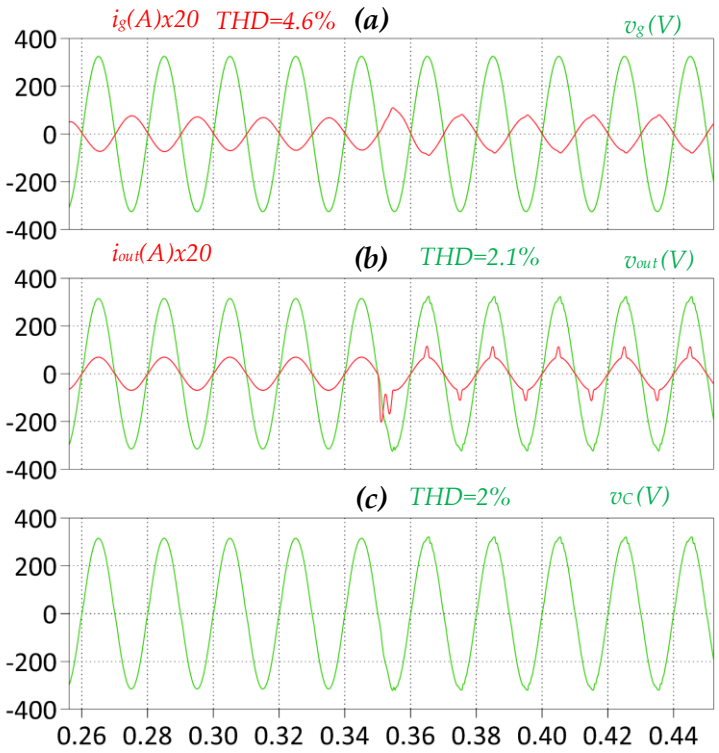

Figure 7. Voltage and current shape at the main grid (a), output (b), and capacitor of the filter with kout = 0, kc = 1.

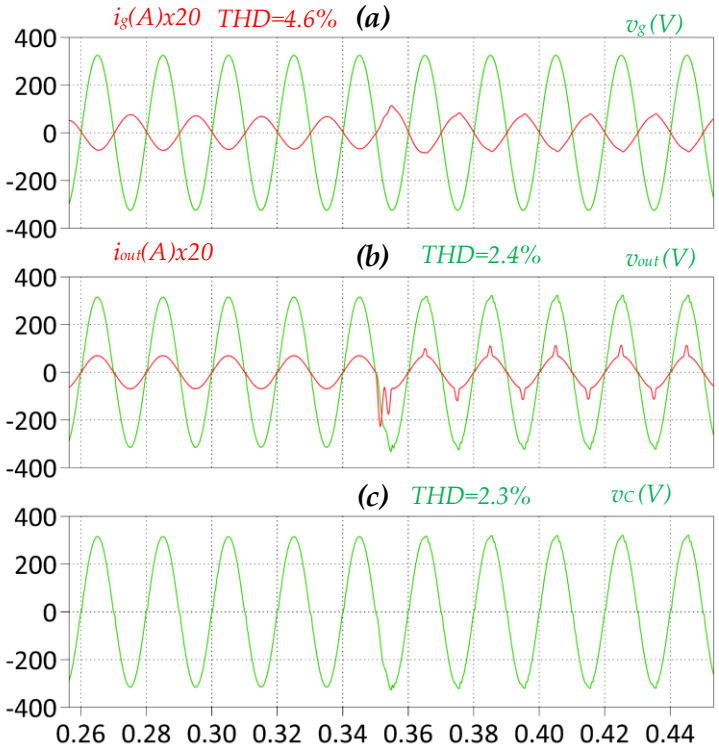

Figure 8. Voltage and current shape at the main grid (a), output (b), and capacitor of the filter with kout = 1, kc = 0.

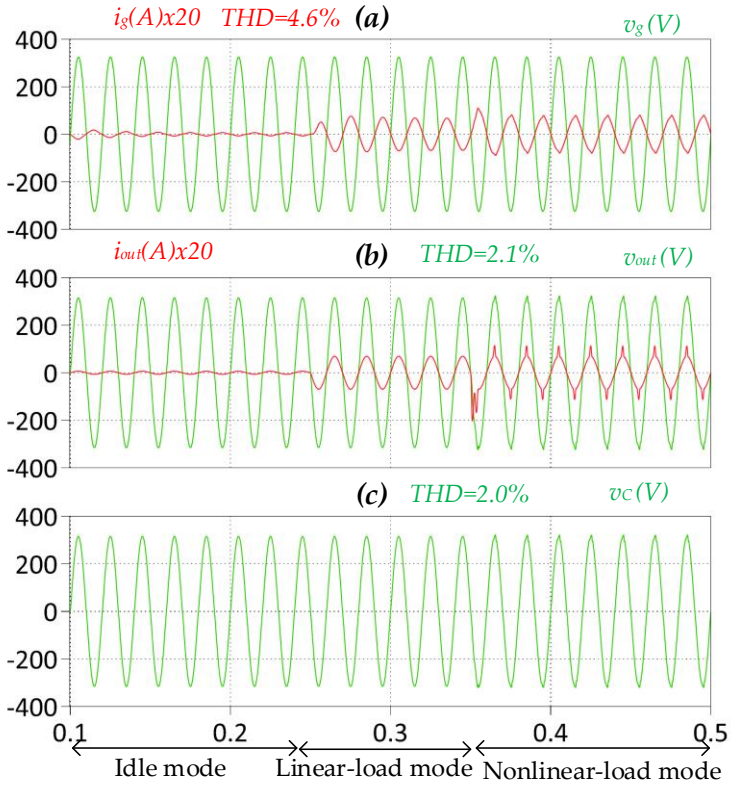

Figure 9. Voltage and current shape transitions at the main grid (a), output (b), and filter capacitor with kout = 0.2 and kc = 0.8 in idle mode, linear load, and nonlinear load.

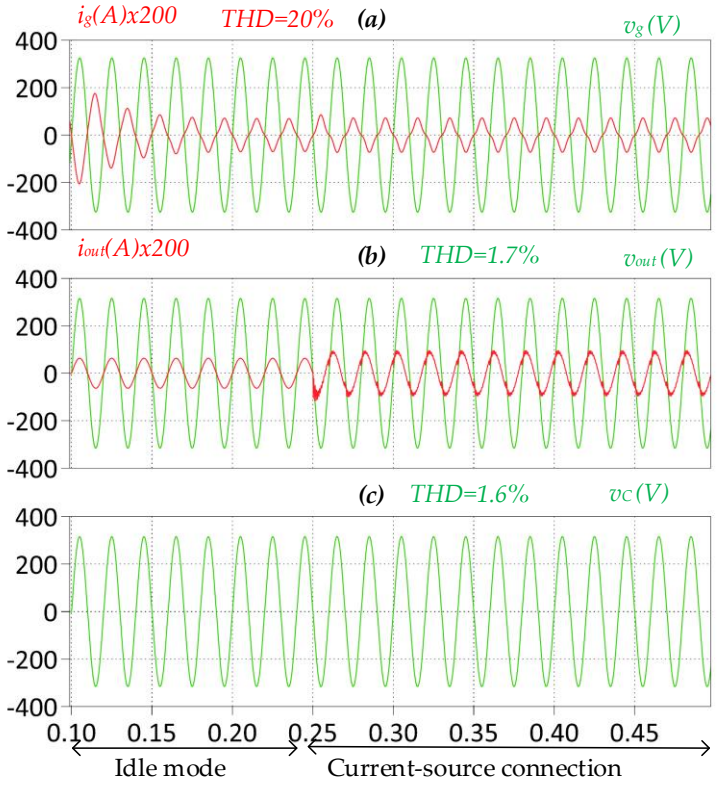

Figure 10. Voltage and current shape transition at the main grid (a), output (b), capacitor of the filter with kout = 0.2, kc = 0.8 in idle mode, and current-source connection.

5. Conclusions

This work studies the energy router based back-to-back inverter in grid forming mode. The conventional PR regulator for grid forming of the energy router has limitations in terms of idle mode, nonlinear loads and current sources. This paper proposes an enhanced iMPC to improve the output voltage quality of the energy router. The tuning procedure and the flow chart control were explained. To improve the THD of the output voltage, a prediction horizon of 2 is suggested. Increasing the number of voltage deviations in each horizon will improve the output voltage quality at the expense of a higher processing burden on the microcontroller at each sampling time. Considering this issue, a voltage deviation of 5, with a total of 25 loops in each sampling time, is implemented on the experimental setup. The experiments were done in four different modes of idle mode, linear load, nonlinear load, and low-power current source connection. The results confirm that the proposed technique can control the steady state and dynamic performance of the energy router in a grid-forming operation.

Author Contributions: Conceptualization: R.S.; Formal analysis: N.S. and M.N.; Validation: M.N. and N.S.; Methodology: O.H.; Visualization M.N., I.R. and K.N.; Investigation: M.N., N.S.; Writing -original draft; M.N. and K.N.; Resources: I.R. and K.S.; Writing – review & editing: R.S. and D.V.; Supervision: D.V. and O.H; Project administration: R.S.; Funding acquisition: N.S. All authors have read and agreed to the published version of the manuscript."

Funding: This research was funded by GDYNIA MARITIME UNIVERSITY, as a part of own research studies in the Department of Ship Automation, Faculty of Electrical Engineering.

Acknowledgments: This research was co-financed by the Estonian Research Council grant PRG675 and by the Estonian Centre of Excellence in Zero Energy and Resource Efficient Smart Buildings and Districts, ZEBE, grant 2020- 2020.4.01.15-0016 funded by the European Regional Development Fund.

Conflicts of Interest: The authors declare no conflict of interest.

References

1. Y. Liu, Y. Fang, and J. Li, "Interconnecting microgrids via the energy router with smart energy management," Energies, vol. 10, no. 9, Aug. 2017, doi: 10.3390/en10091297.
2. A. Q. Huang et al., "The future renewable electric energy delivery and management (FREEDM) system: The energy internet," Proc. IEEE, vol. 99, no. 1, pp. 133–148, Jan. 2011, doi: 10.1109/JPROC.2010.2081330.
3. J. F. Martins, E. Romero-Cadaval, D. Vinnikov, and M. Malinowski, "Transactive Electronics Power Energy: Challenges," no. February, pp. 20–32, 2022.
4. R. Fu, T. Remo, R. Margolis, R. Fu, T. Remo, and R. Margolis, "2018 U . S . Utility-Scale Photovoltaics- Plus-Energy Storage System Costs Benchmark," 2018. [Online]. Available: https://www.nrel.gov/docs/fy19osti/71714.pdf.%0Ahttps://www.nrel.gov/docs/fy19osti/71714.pdf.
5. Yingpei Liu, Y. Li, H. Liang, J. He, and H. Cui, "Energy Routing Control Strategy for Integrated Microgrids Including Photovoltaic, Battery-Energy Storage and Electric Vehicles," energies Artic., 2019, doi: 10.3390/en12020302.
6. O. Ray and S. Mishra, "Integrated Hybrid Output Converter as Power Router for Renewable-based Nanogrids," in IECON2015-Yokohama, 2015, pp. 1645–1650.
7. Li Zhen; Li Penghua; Sheng Wanxing; Du Songhuai; Duan Qing; Lv Zhipeng, "Research on a household energy router for energy internet," Proc. 13th IEEE Conf. Ind. Electron. Appl. ICIEA 2018, no. 17, pp. 952–957, 2018, doi: 10.1109/ICIEA.2018.8397849.
8. M. Hagh Tarafdar and F. Hamzeh Aghdam, "Smart Hybrid Nanogrids Using Modular Multiport Power Electronic Interface," in 2016 IEEE Innovative Smart Grid Technologies - Asia (ISGT-Asia), 2016, pp. 11–16.
9. S. Mishra and O. Ray, "Advances in nanogrid technology and its integration into rural electrification in India," 2014 Int. Power Electron. Conf. IPEC-Hiroshima - ECCE Asia 2014, no. c, pp. 2707–2713, 2014, doi: 10.1109/IPEC.2014.6869973.
10. R. Majumder, "A hybrid microgrid with dc connection at back to back converters," IEEE Trans. Smart Grid, vol. 5, no. 1, pp. 251–259, Jan. 2014, doi: 10.1109/TSG.2013.2263847.
11. M. Najafzadeh, O. Husev, I. Roasto, and T. Jalakas, "Improved DC-Link Voltage Transient Response and Stability Issues in Energy Router with Fuzzy Logic Control Method."
12. I. Roasto, A. Rosin, and T. Jalakas, "Multiport Interface Converter with an Energy Storage for Nanogrids," IECON 2018 - 44th Annu. Conf. IEEE Ind. Electron. Soc., vol. 1, pp. 6088–6093.
13. M. Najafzadeh, I. Roasto, and T. Jalakas, "Energy Router Based Energy Management System for Nearly Zero Energy Buildings," 2019.

14. Y. Yang, L. Hadjidemetriou, F. Blaabjerg, and E. Kyriakides, "Benchmarking of Phase Locked Loop based Synchronization Techniques for Grid-Connected Inverter Systems," in 9th International Conference on Power Electronics-ECCE Asia, 2015, pp. 2167–2174.
15. O. Husev, C. Roncero-Clemente, E. Makovenko, S. P. Pimentel, D. Vinnikov, and J. Martins, "Optimization and Implementation of the Proportional-Resonant Controller for Grid-Connected Inverter with Significant Computation Delay," IEEE Trans. Ind. Electron., vol. 67, no. 2, pp. 1201–1211, 2020, doi: 10.1109/TIE.2019.2898616.
16. J. Rocabert, A. Luna, F. Blaabjerg, and Pedro Rodr´ıguez, "Control of Power Converters in AC Microgrids," vol. 27, no. 11, pp. 4734–4749, 2012.
17. M. J. A. J. Hossain, H. R. Pota, W. Issa, and M. J. A. J. Hossain, "Overview of AC microgrid controls with inverter-interfaced generations," Energies, vol. 10, no. 9, pp. 1–27, 2017, doi: 10.3390/en10091300.
18. E. Unamuno and J. A. Barrena, "Hybrid ac/dc microgrids - Part II: Review and classification of control strategies," Renew. Sustain. Energy Rev., vol. 52, pp. 1123–1134, Aug. 2015, doi: 10.1016/j.rser.2015.07.186.
19. S. M. Malik, X. Ai, Y. Sun, C. Zhengqi, and Z. Shupeng, "Voltage and frequency control strategies of hybrid AC/DC microgrid: a review," IET Gener. Transm. Distrib., vol. 11, no. 2, pp. 303–313, Jan. 2017, doi: 10.1049/iet-gtd.2016.0791.
20. P. C. Loh, D. Li, Y. K. Chai, and F. Blaabjerg, "Autonomous control of interlinking converter with energy storage in hybrid AC-DC microgrid," IEEE Trans. Ind. Appl., vol. 49, no. 3, pp. 1374–1382, 2013, doi: 10.1109/TIA.2013.2252319.
21. U. B. Tayab, M. A. Bin Roslan, L. J. Hwai, and M. Kashif, "A review of droop control techniques for microgrid," Renew. Sustain. Energy Rev., vol. 76, no. May 2016, pp. 717–727, 2017, doi: 10.1016/j.rser.2017.03.028.
22. J. M. Guerrero, L. G. De Vicuña, J. Matas, and M. Castilla, "Output Impedance Design of Parallel-Connected UPS Inverters With Wireless Load-Sharing Control," IEEE Trans. Ind. Electron., vol. 52, no. 4, pp. 1126–1135, 2005.
23. H. Zhang, J. Zhou, Q. Sun, J. M. Guerrero, and D. Ma, "Data-Driven Control for Interlinked AC/DC Microgrids Via Model-Free Adaptive Control and Dual-Droop Control," IEEE Trans. Smart Grid, vol. 8, no. 2, pp. 557–571, 2017, doi: 10.1109/TSG.2015.2500269.
24. H. Mahmood, D. Michaelson, and J. Jiang, "Decentralized Power Management of a PV/Battery Hybrid Unit in a Droop-Controlled Islanded Microgrid," IEEE Trans. Power Electron., vol. 30, no. 12, pp. 7215–7229, 2015, doi: 10.1109/TPEL.2015.2394351.
25. J. Wang, C. Dong, C. Jin, P. Lin, and P. Wang, "Distributed Uniform Control for Parallel Bidirectional Interlinking Converters for Resilient Operation of Hybrid AC/DC Microgrid," IEEE Trans. Sustain. Energy, vol. 13, no. 1, pp. 3–13, 2022, doi: 10.1109/TSTE.2021.3095085.
26. J. He, Y. W. Li, J. M. Guerrero, F. Blaabjerg, and J. C. Vasquez, "An Islanding Microgrid Power Sharing Approach Using Enhanced Virtual Impedance Control Scheme," IEEE Trans. Power Electron., vol. 28, no. 11, pp. 5272–5282, 2013.
27. X. yan Jiang, C. He, and K. Jermsittiparsert, "Online optimal stationary reference frame controller for inverter interfaced distributed generation in a microgrid system," Energy Reports, vol. 6, pp. 134–145, Nov. 2020, doi: 10.1016/j.egyr.2019.12.016.
28. Q. C. Zhong and G. Weiss, "Synchronverters: Inverters that mimic synchronous generators," IEEE Trans. Ind. Electron., vol. 58, no. 4, pp. 1259–1267, Apr. 2011, doi: 10.1109/TIE.2010.2048839.
29. J. Liu, M. J. Hossain, J. Lu, F. H. M. Rafi, and H. Li, "A hybrid AC/DC microgrid control system based on a virtual synchronous generator for smooth transient performances," Electr. Power Syst. Res., vol. 162, no. March, pp. 169–182, Sep. 2018, doi: 10.1016/j.epsr.2018.05.014.
30. C. Arghir, T. Jouini, and F. Dörfler, "Grid-forming control for power converters based on matching of synchronous machines," Elsevier Autom., vol. 95, pp. 273–282, 2018, doi: 10.1016/j.automatica.2018.05.037.
31. J. Rodriguez, J. Kolar, J. Espinoza, M. Rivera, and C. Rojas, "Predictive Torque and Flux Control of an Induction Machine fed by an Indirect Matrix Converter with Reactive Power Minimization," in 2010 IEEE International Symposium on Industrial Electronics, 2010, pp. 3177–3183.
32. R. Kennel and A. Linder, "Predictive control of inverter supplied electrical drives," in 2000 IEEE 31st Annual Power Electronics Specialists Conference. Conference Proceedings (Cat. No.00CH37018), 2000, vol. 00, no. c, pp. 761–766.
33. Zhuikov V., Pavlov V., Strzelecki R.G. Preemptive control systems for valve converters. – K.: Nauk. Dumka, 1991. - 240 p.
34. J. Rodriguez et al., "State of the art of finite control set model predictive control in power electronics," IEEE Trans. Ind. Informatics, vol. 9, no. 2, pp. 1003–1016, May 2013, doi: 10.1109/TII.2012.2221469.
35. P. Falkowski and A. Sikorski, "Finite Control Set Model Predictive Control for Grid-Connected AC – DC Converters With LCL Filter," IEEE Trans. Ind. Electron., vol. 65, no. 4, pp. 2844–2852, 2018.
36. D. Wojciechowski; R. Strzelecki, "Sensorless predictive control of three-phase parallel active filter", in Proc. of AFRICON 2007.
37. . Hu, Y. Shan, J. M. Guerrero, A. Ioinovici, K. W. Chan, and J. Rodriguez, "Model predictive control of microgrids – An overview," Renew. Sustain. Energy Rev., vol. 136, no. October 2020, 2021, doi: 10.1016/j.rser.2020.110422.
38. S. Kouro, M. A. Perez, J. Rodriguez, A. M. Llor, and H. A. Young, "Model Predictive Control: MPC's Role in the Evolution of Power Electronics," IEEE Ind. Electron. Mag., vol. 9, no. 4, pp. 8–21, 2015, doi: 10.1109/MIE.2015.2478920.
39. M. Wojciechowski, R. Strzelecki, G. Benysek, "Predictive Control System of the Shunt Active Power Filter" In proc. of 2008 International Biennial Baltic Electronics Conference (BEC2008) Tallinn, Estonia, October 6-8, 2008.
40. D. Wojciechowski, R. Strzelecki, "Predictive Control of Active Filter System with LCL Coupling Circuit", In proc. of the 2010 International Power Electronics Conference, 2010.

41. J. Lee, J. Lee, H. Moon, and K. Lee, "An Improved Finite-Set Model Predictive Control Based on Discrete Space Vector Modulation Methods for Grid-Connected Three-Level Voltage Source Inverter," IEEE J. Emerg. Sel. Top. Power Electron., vol. 6, no. 4, pp. 1744–1760, 2018.
42. F. Wang, H. Xie, Q. Chen, S. A. Davari, J. Rodríguez, and R. Kennel, "Parallel Predictive Torque Control for Induction Machines Without Weighting Factors," IEEE Trans. POWER Electron., vol. 35, no. 2, pp. 1779–1788, 2020.
43. Roasto, I.; Husev, O.; Najafzadeh, M.; Jalakas, T.; Rodriguez, J., "Voltage Source Operation of the Energy-Router Based on Model Predictive Control," Energies, vol. 12, no. 10, p. 1892, 2019, doi: 10.3390/en12101892.